Yolk-Shell type Carbon-Silica Nanoarchitecture Dispersed and Stabilized Ru Nanoparticles for Enhanced Hydrogenation of Aromatic Compounds

Lu Yan,‡[a,b] Yue Shen,‡[a,b] Zidan Zou,[a,b] Xiao Zhang,[*a] Zhixin Yu,[c] Guozhong Wang,[a,b] Chun Chen,[*a,b]

[a] Key Laboratory of Materials Physics, Centre for Environmental and Energy Nanomaterials, Key Laboratory of Materials Physics, Institute of Solid State Physics, HFIPS, Chinese Academy of Sciences, Hefei, 230031, China.

[b] Science Island Branch, Graduate School of USTC, Hefei, 230026, China.

[c] Department of Petroleum Engineering, University of Stavanger, Stavanger 4036, Norway.

‡ These authors contributed equally to this work.

Corresponding Author: X. Zhang (zhangxiao@issp.ac.cn), C. Chen (chenchun2013@issp.ac.cn)
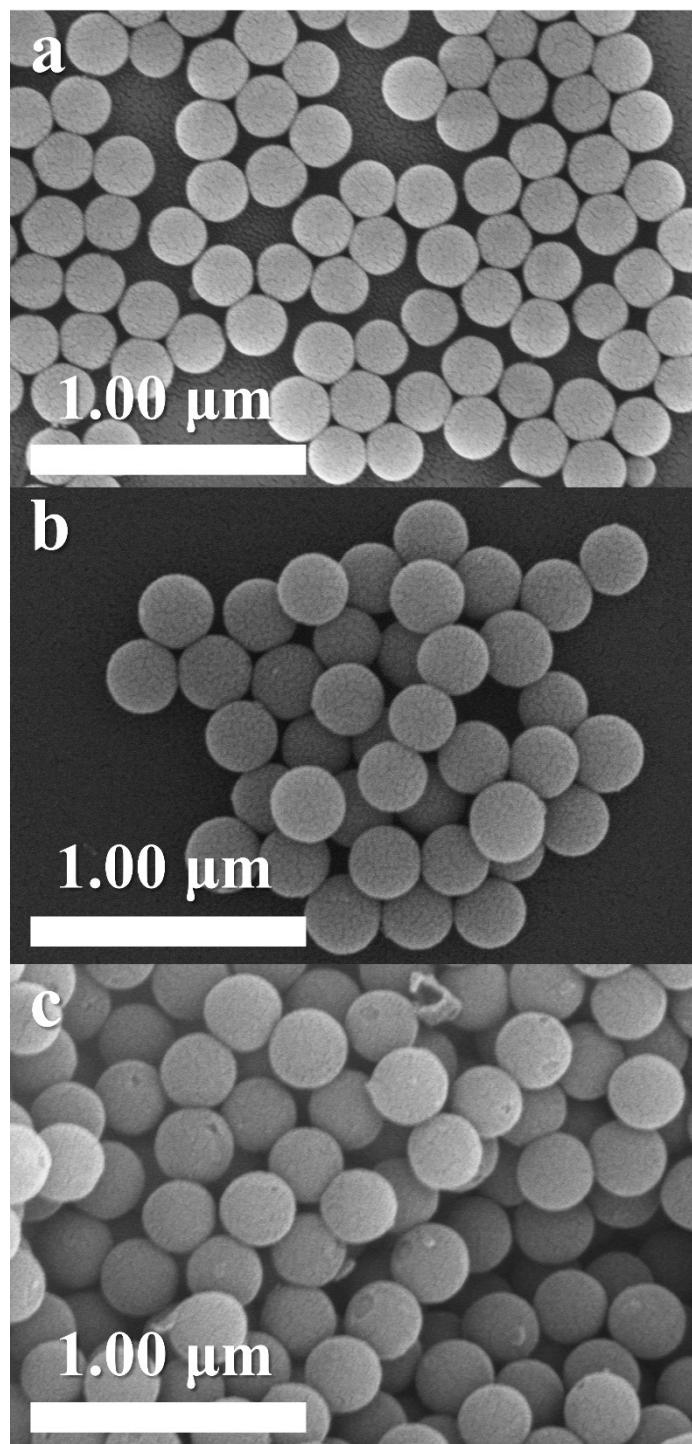
Fig. S1. SEM images of **(a)** SiO$_2$, **(b)** SiO$_2$@NC, and **(c)** SiO$_2$@void@NC.
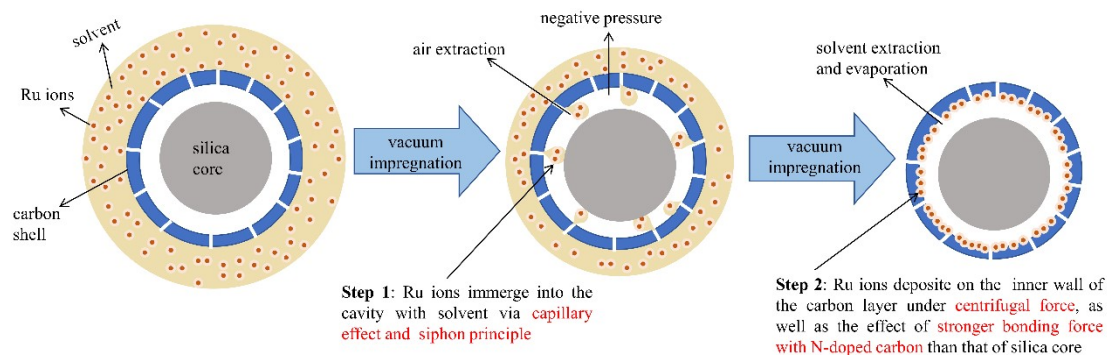
Fig. S2. The mechanism of Ru loaded onto the SiO$_2$@void@NC under vacuum assisted impregnation method.

In the process of vacuum impregnation, air overflows from the cavity, forming a pressure difference inside and outside the carbon layer, and metal ions enter the cavity with solvent through the mesoporous pore channels under the effect of capillary action. Further, with the evaporation of the solvent, a siphon effect is produced, in which the solvent brings all the metal ions into the cavity and deposits them in the cavity as the solvent evaporates from the pore. During this process, most metal ions adhere to the inner wall of carbon layer due to the centripetal force and strong interaction with nitrogen-doped carbon, and a small amount of metal ions are deposited on the surface of silica. Because the core silica is mobile in the cavity after etching, the core of silica constantly collides with the inner wall of the carbon layer during the process of rotary evaporation. The metal ions deposited on the surface of silica are trapped by the carbon layer due to their stronger bonding force with nitrogen-doped carbon. Eventually, almost all of the metal ions attach to the inner wall of the carbon layer.
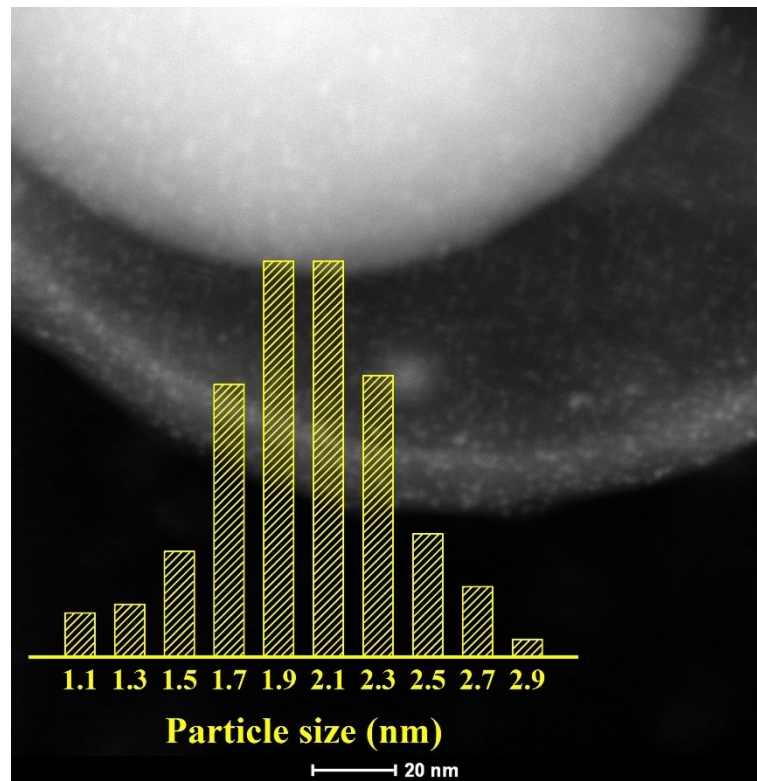
**Fig. S3.** HADDF-STEM image and Ru particle size distribution of SiO$_2$@Ru@NC.
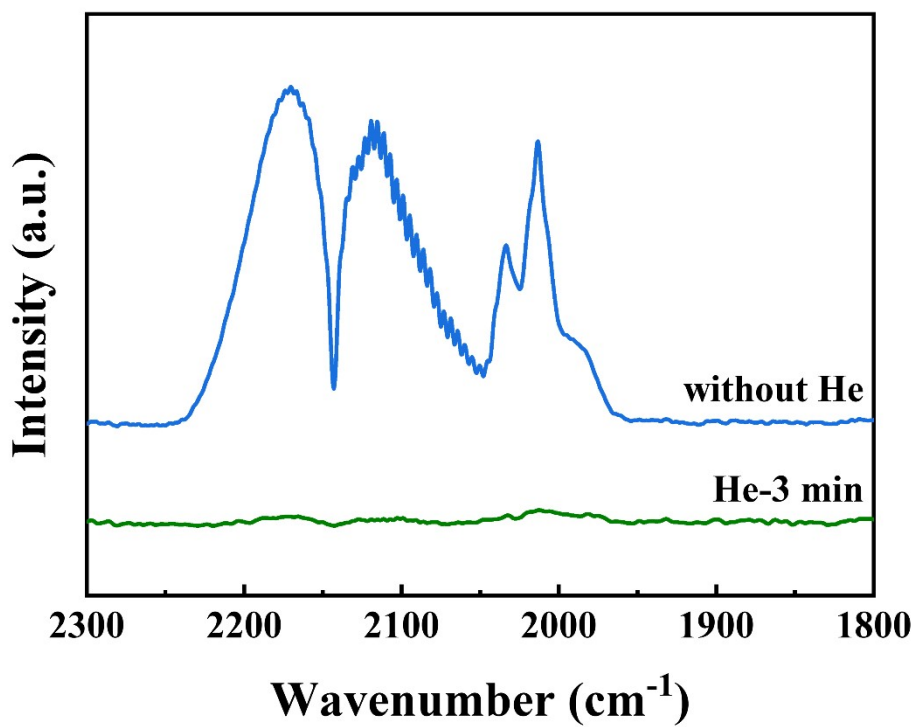
Fig. S4. CO-DRIFTS of SiO$_2$@Ru@NC: without helium blowing (Without He) and helium blowing for 3 minutes (He-3 min).
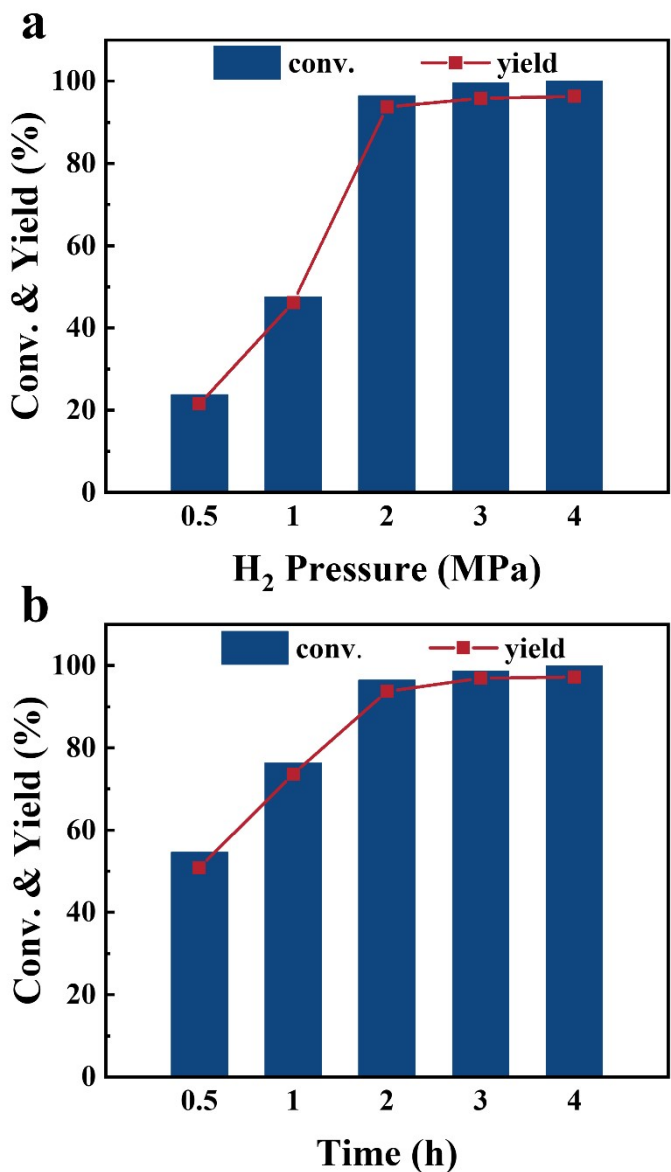
Fig. S5. (a) Effect of H_2 pressure, 40 mg catalysts, 200 mg DMT, 90 °C, 10 mL methanol, 2 h; **(b)** Effect of reaction time, 40 mg catalysts, 200 mg DMT, 2 MPa H_2, 90 °C, 10 mL methanol.
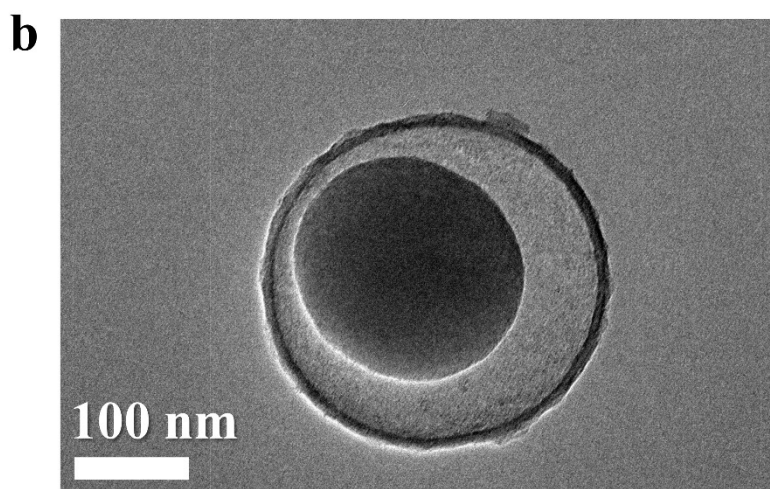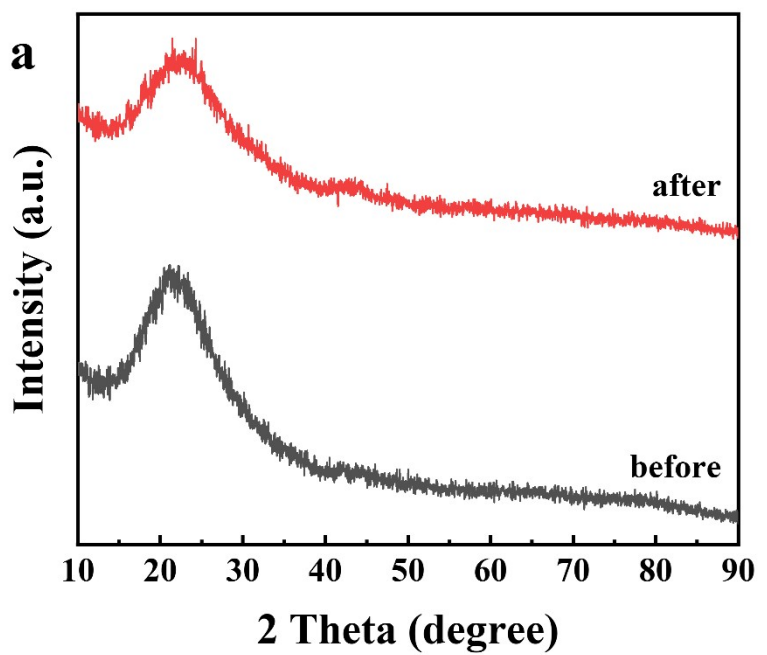
Fig. S6. (a) XRD before and after 5 cycles, **(b)** TEM after 5 cycles of SiO$_2$@Ru@NC.
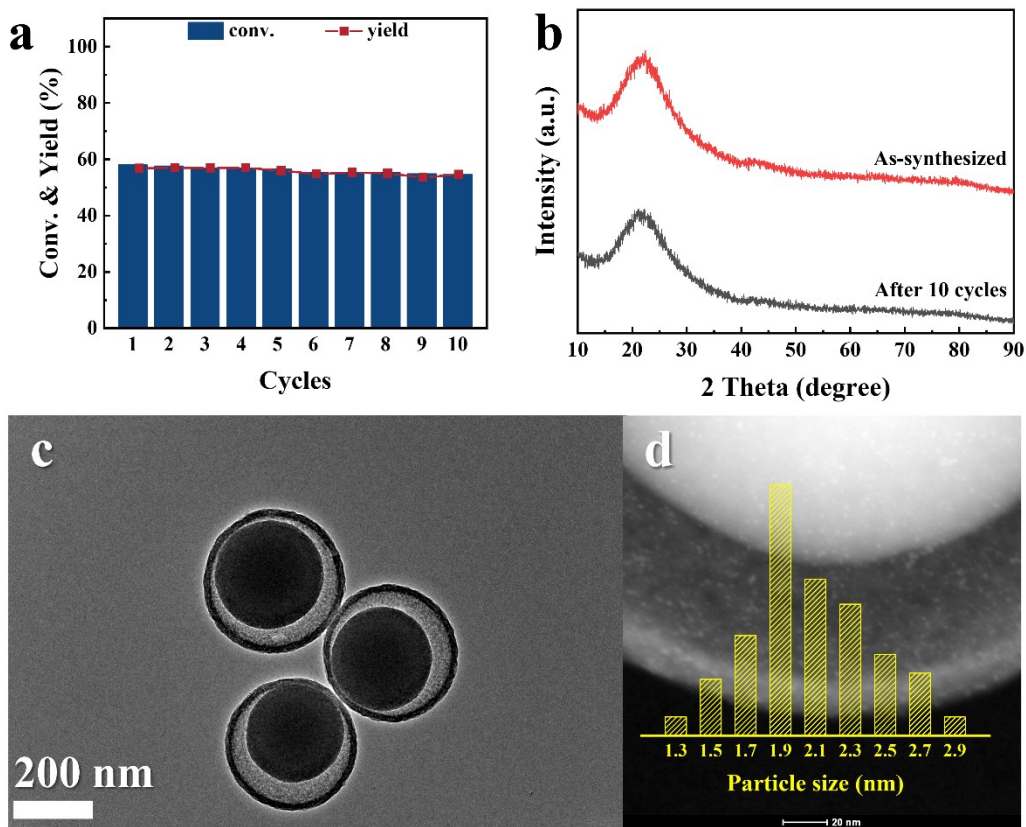
Fig. S7. (a) Performance of 10 cycles. Reaction conditions: 40 mg catalysts, 200 mg DMT, 2 MPa H_2, 90 °C, 10 mL methanol, 0.5 h per cycle; (b) XRD of the as-synthesized SiO$_2$@Ru@NC and SiO$_2$@Ru@NC after 10 cycles; (c) TEM, (d) HADDF-STEM image and Ru particle size distribution of SiO$_2$@Ru@NC after 10 cycles.
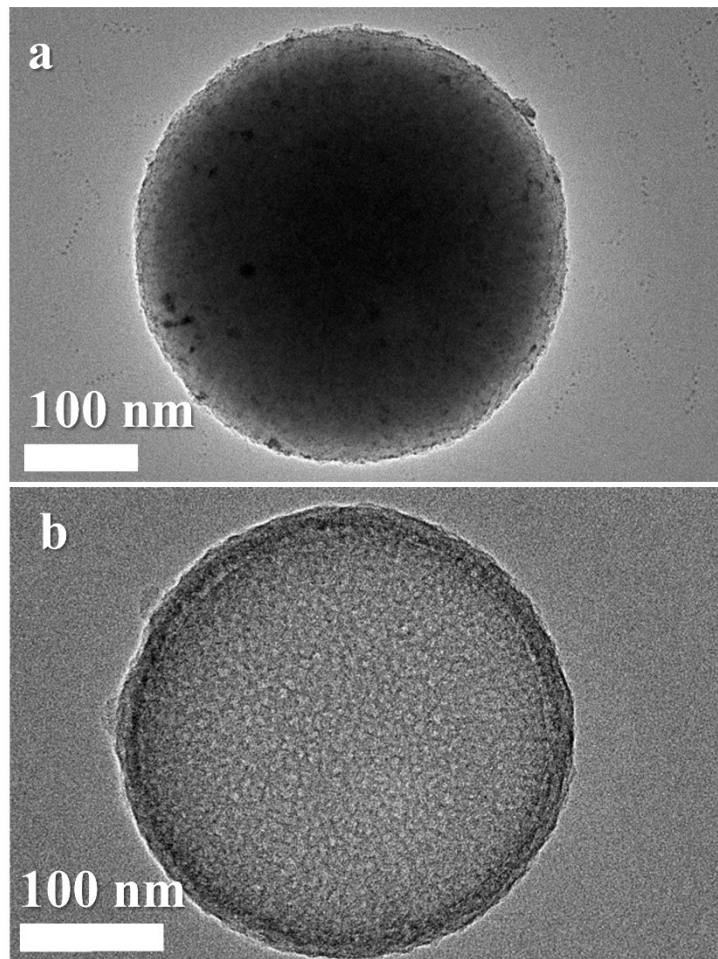
Fig. S8. TEM of **(a)** Ru/SiO$_2$@NC and **(b)** Ru@HCS.
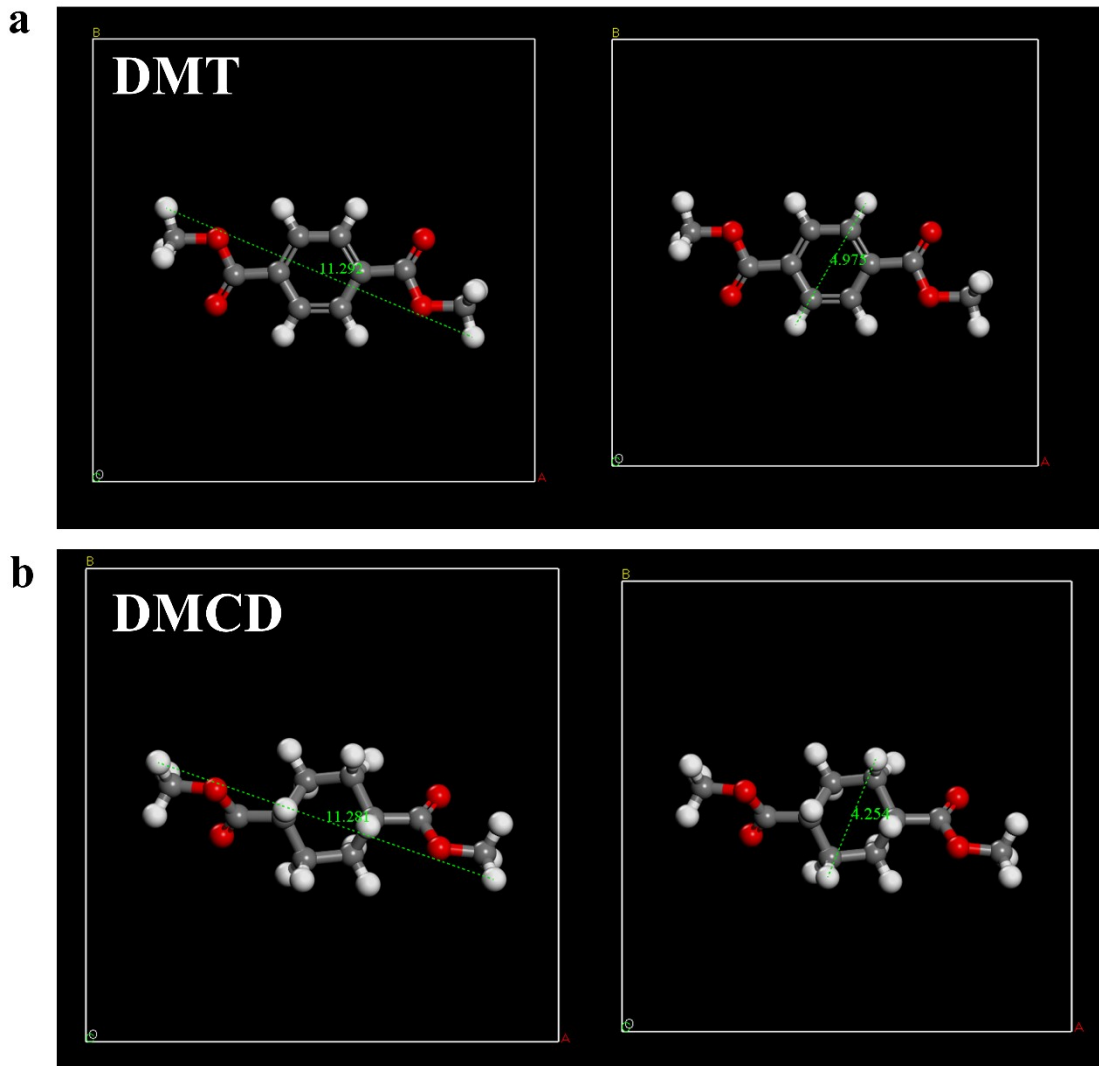
Fig. S9. The plane size of **(a)** DMT, **(b)** DMCD.
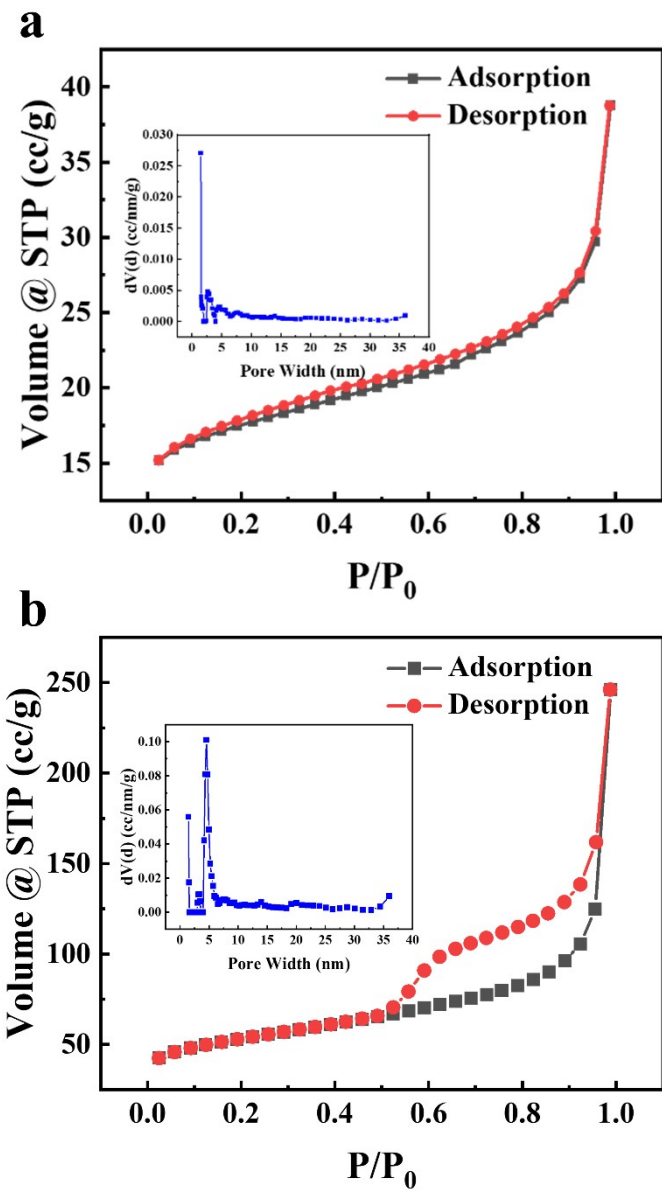
Fig. S10. Nitrogen adsorption-desorption isotherm and DFT pore size distributions of **(a)** SiO_2@NC and

(b) HCS.
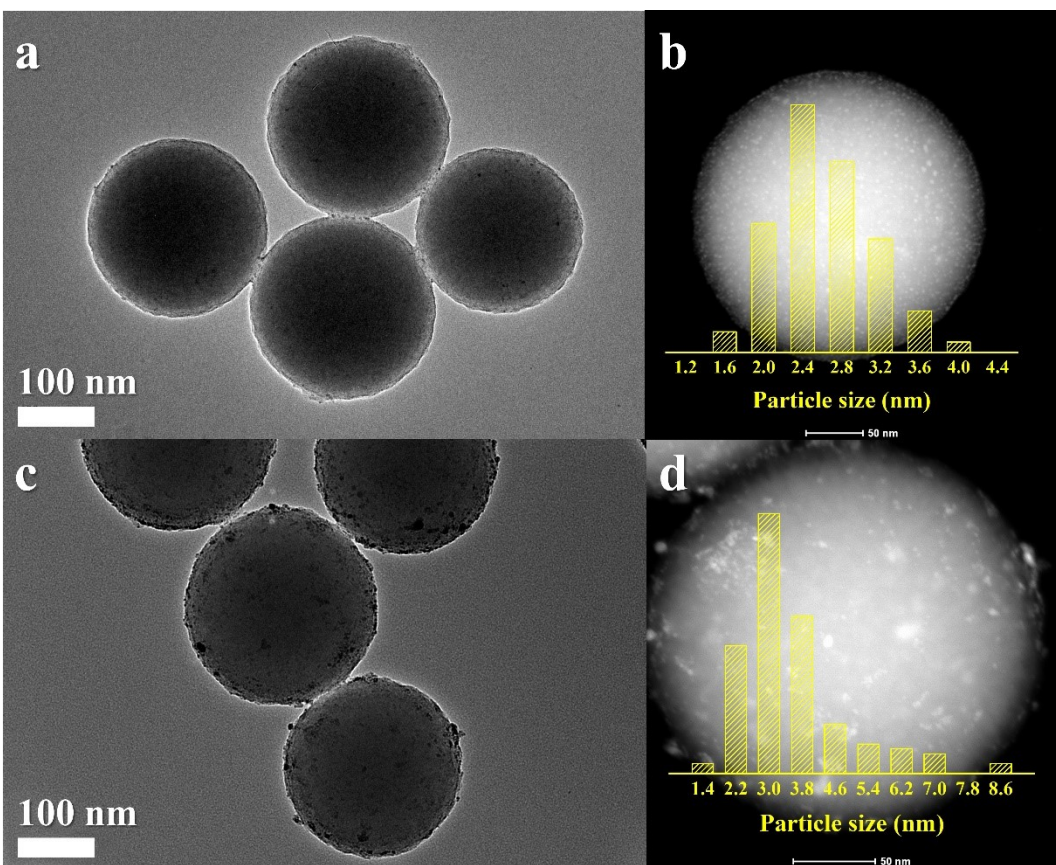
Fig. S11. (a) TEM, **(b)** HADDF-STEM image and Ru particle size distribution of as-synthesized

Ru/SiO$_2$@NC; **(c)** TEM, **(d)** HADDF-STEM image and Ru particle size distribution of Ru/SiO$_2$@NC after 3

cycles.
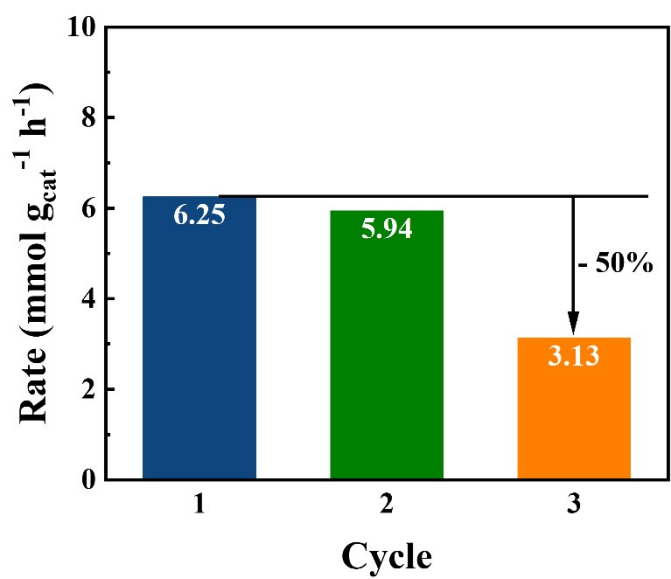
Fig. S12. Reaction rate of Ru/CAC catalyst.
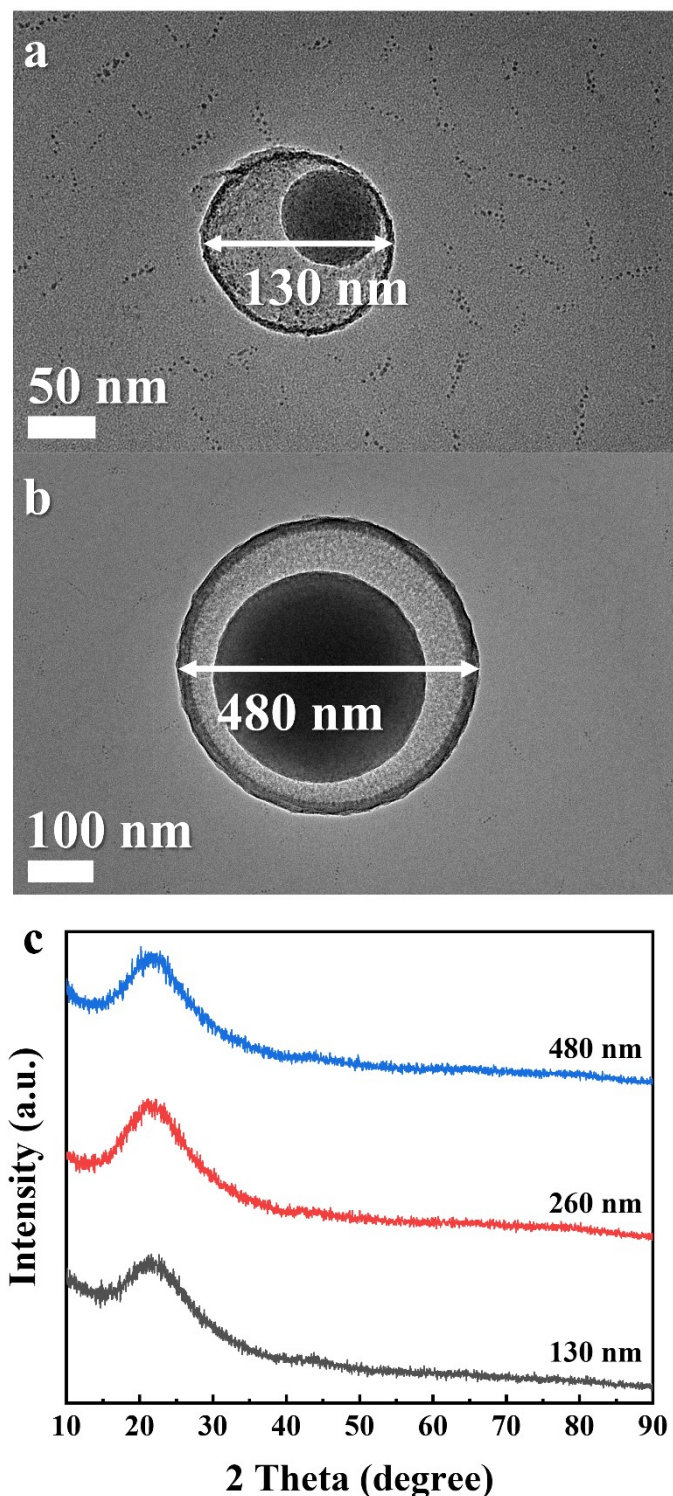
Fig. S13. **(a)(b)** TEM and **(c)**XRD patterns of SiO$_2$@Ru@NC with different sizes.
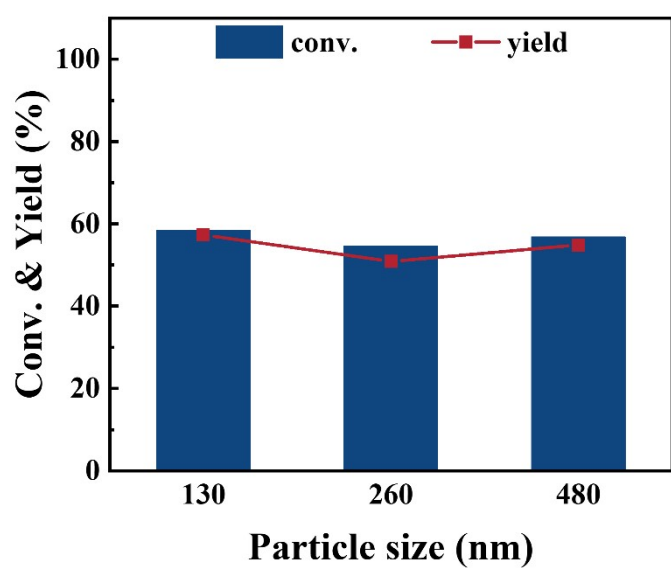
Fig. S14. Effect of the size on the catalytic activity. Reaction conditions: 40 mg catalysts, 200 mg DMT,

2 MPa H_2, 90 °C, 10 mL methanol, 0.5 h.
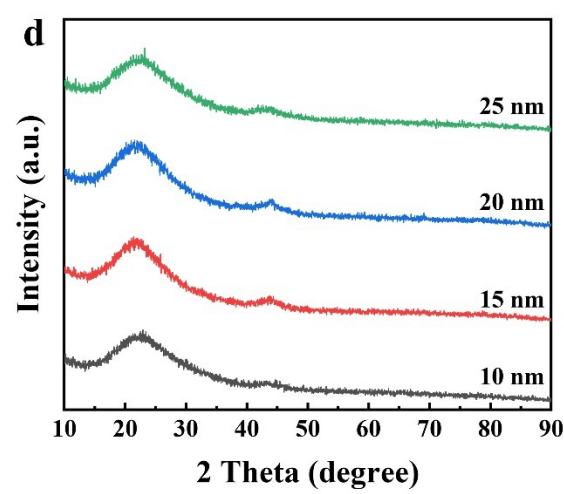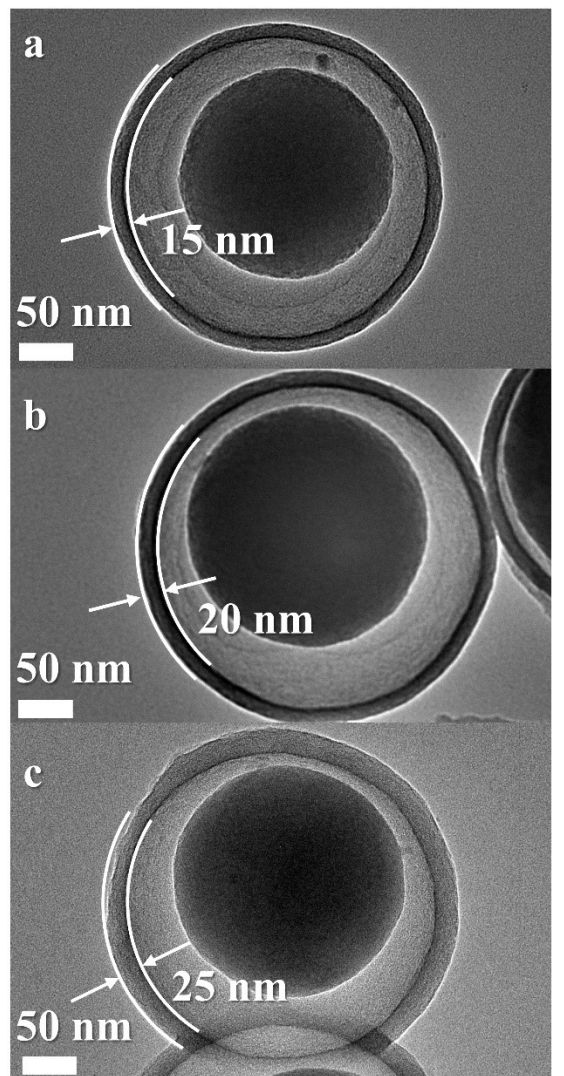
Fig. S15. (a)(b)(c) TEM and **(d)** XRD patterns of SiO$_2$@Ru@NC with different thickness of the carbon
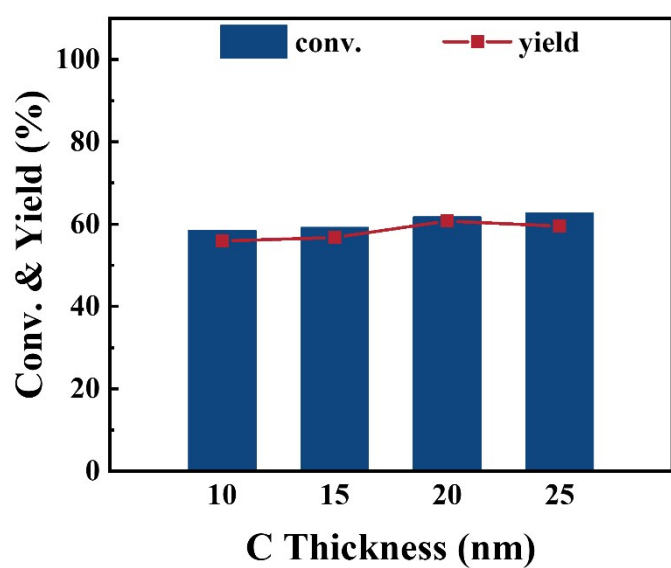
layer.

Fig. S16. Effect of the thickness of the carbon layer on the catalytic activity. Reaction conditions: 40 mg catalysts, 200 mg DMT, 2 MPa H_2, 90 °C, 10 mL methanol, 0.5 h.
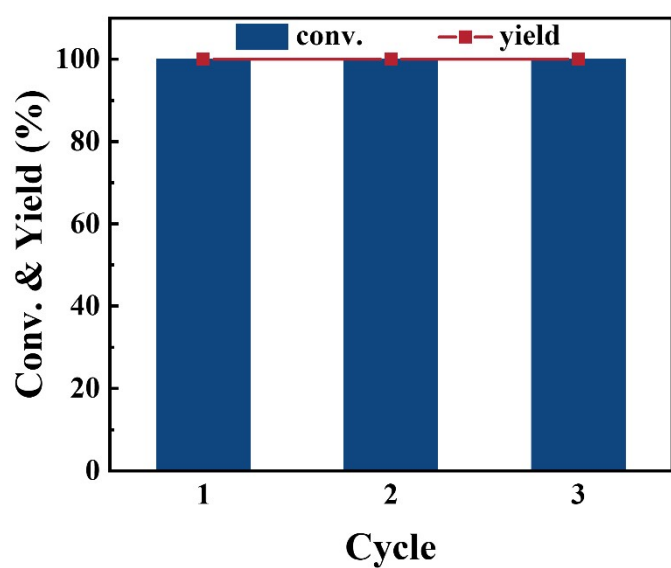
Fig. S17. Cycle stability test in aqueous phase. Reaction conditions: 40 mg catalysts, 200 mg DMT, 2 MPa H_2, 90 °C, 10 mL H_2O, 4 h.
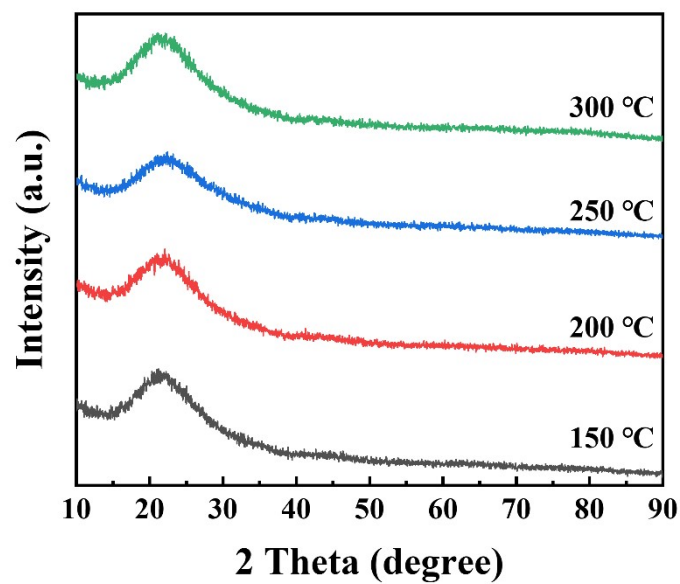
Fig. S18. XRD of SiO$_2$@Ru@NC at different reduction temperatures.
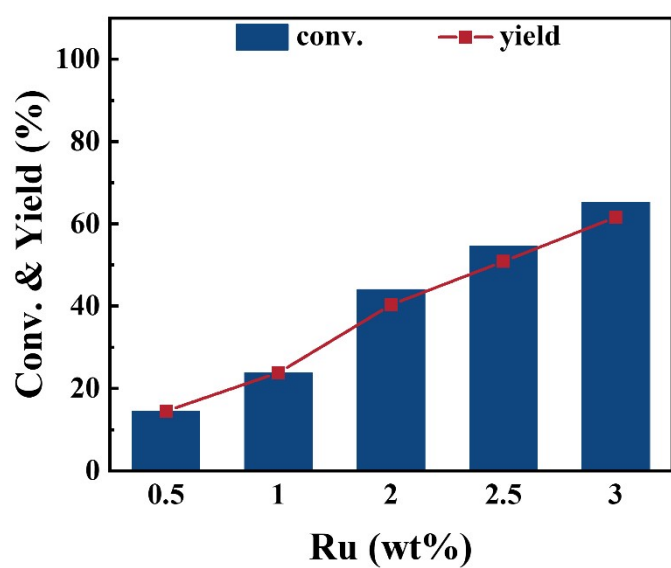
Fig. S19. Effect of Ru loading on the catalytic activity. Reaction conditions: 40 mg catalysts, 200 mg

DMT, 2 MPa H_2, 90 °C, 10 mL methanol, 0.5 h.

a

18.26°
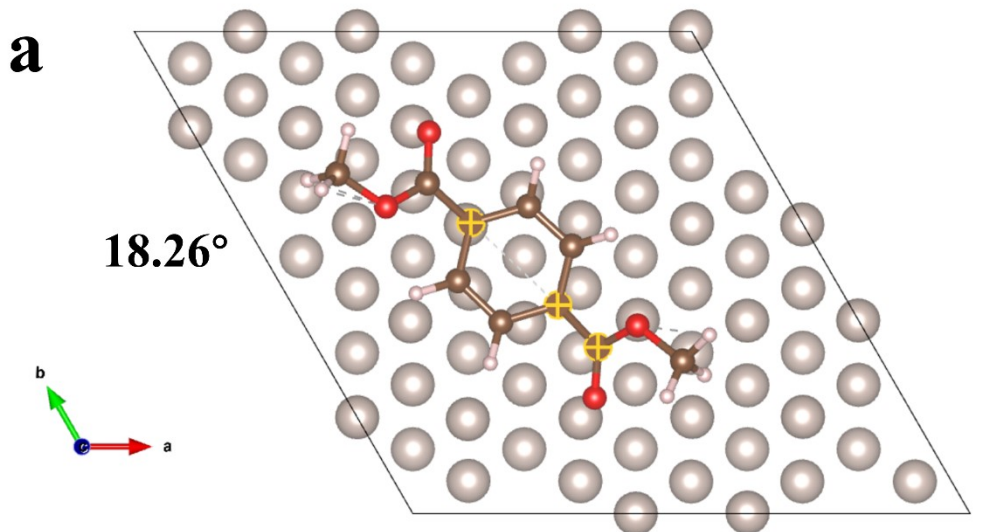
(x,y,z):   1.41005   7.06201   8.42062
          Occ. = 1.000   Ueq = 0.00000   la   l

phi(C8-C4-C1) = 161.7392(0) deg.
 18   C8 C   0.50511 0.34522 0.36120 (0, 0, 0)+ x, y, z
 14   C4 C   0.47640 0.43237 0.34321 (0, 0, 0)+ x, y, z
 11   C1 C   0.40571 0.60292 0.34486 (0, 0, 0)+ x, y, z

b

13.83°
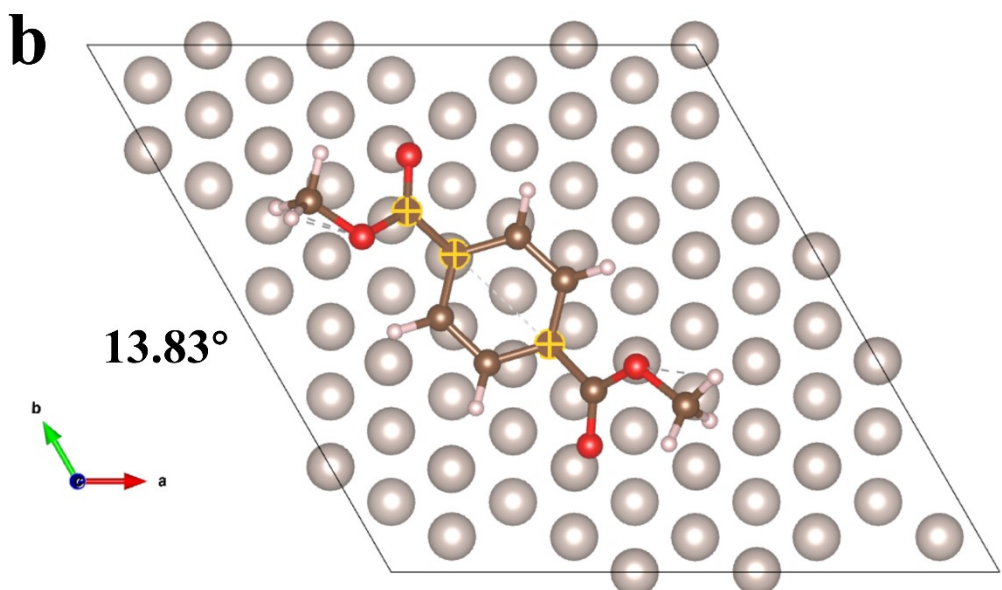
(x,y,z):   3.51941   5.06441   8.38037
          Occ. = 1.000   Ueq = 0.00000   la   l

phi(C7-C1-C4) = 166.1677(0) deg.
 17   C7 C   0.36864 0.68500 0.36008 (0, 0, 0)+ x, y, z
 11   C1 C   0.40571 0.60292 0.34486 (0, 0, 0)+ x, y, z
 14   C4 C   0.47640 0.43237 0.34321 (0, 0, 0)+ x, y, z

Fig. S20. DFT calculation of the angle between the six membered ring and the ester group on **(a)** DMT,

(b) DMCD.

Table S1. The XPS testing of element content in different catalysts.

Name	XPS Atomic %			
	SiO$_2$@Ru@NC	Ru/AC	Ru/Al$_2$O$_3$	Ru/SiO$_2$
C	87.51	87.71	16.23	7.75
Si	1.57	0.6	0	29.73
N	2.13	0.95	0.71	0.96
Ru	0.5	0.32	0.65	0.52
O	8.3	10.42	82.41	61.03

Table S2. The ICP-AES of samples with different Ru loadings.

Simple	ICP-AES result (wt %)
SiO_2@0.5%Ru@NC	0.46
SiO_2@1.0%Ru@NC	0.97
SiO_2@2.0%Ru@NC	1.89
SiO_2@2.5%Ru@NC	2.30
SiO_2@3.0%Ru@NC	2.63
SiO_2@2.5%Ru@NC-after 5 cycles	2.14
SiO_2@2.5%Ru@NC-after 3 cycles	2.23
2.5%Ru/SiO_2@NC	2.39
2.5%Ru/SiO_2@NC-after 3 cycles	1.54
2.5%Ru@HCS	2.20
2.5%Ru@HCS-after 3 cycles	2.06
2.5%Ru/CAC	2.36
2.5%Ru/CAC-after 3 cycles	1.92
SiO_2@2.5%Ru@NC-after 10 cycles	2.08

Table S3. Comparison of reaction conditions for aromatic ring hydrogenation.

Entry	Catalyst	Reaction conditions			Conversion of reactants containing aromatic rings (%)	Yield of selective hydrogenation products of aromatic rings (%)
		Temperature (°C)	H_2 Pressure (MPa)	Time (h)		
1	Ru/CeO$_2$–S[1]	200-250	1	6-12	99.9	99.9
2	Ru-B alloy[2]	60	7	2.5	/	99.3
3	1.5Ru1.5Pd[3]	180	8	6	88.5	85.1
4	Ru$_5$/Al$_{20}$SBA-15[4]	100	4.14	1	93.4	93.4
5	Ru/h-BN[5]	130	5	5	100	99.9
6	Ru/g-C$_3$N$_4$-H$_2$[6]	130	5	1	100	> 99
7	Ru−Ni/CNT[7]	150	5	1	80	76
8	CoO$_x$@CN[8]	150	3	16	98	98
9	Co-PMA-PZ@SiO$_2$[9]	135	5	24	/	95
10	Ni/SiO$_2$-AEH[10]	140	3	5	> 99	95.5
This work	SiO$_2$@Ru@NC	90	2	4	100	97.2

Reference:

1 K. Zhang, Q. Meng, H. Wu, J. Yan, X. Mei, P. An, L. Zheng, J. Zhang, M. He and B. Han, Selective Hydrodeoxygenation of Aromatics to Cyclohexanols over Ru Single Atoms Supported on CeO_2, *J. Am. Chem. Soc.*, 2022, **144**, 20834-20846.

2 Q. Pei, J. Yu, G. Qiu, K. C. Tan, J. Wen, Y. Yu, J. Wang, J. Guo, J. Guo, L. Rao, T. He and P. Chen, Fabrication of ultrafine metastable Ru-B alloy for catalytic hydrogenation of NEC at room temperature, *Appl. Catal. B-Environ.*, 2023, **336**, 122947.

3 J. Chen, X. Liu and F. Zhang, Composition regulation of bimetallic RuPd catalysts supported on porous alumina spheres for selective hydrogenation, *Chem. Eng. J.*, 2015, **259**, 43-52.

4 W. Yu, S. Bhattacharjee, W.-Y. Lu and C.-S. Tan, Synthesis of Al-Modified SBA-15-Supported Ru Catalysts by Chemical Fluid Deposition for Hydrogenation of Dimethyl Terephthalate in Water, *Acs Sustain. Chem. Eng.*, 2020, **8**, 4058-4068.

5 Z. Han, L. Wang, Y. Cao, S. Xu, J. Wu, X. Wang, P. He, H. Liu and H. Li, Highly Dispersed Ru Nanoclusters Anchored on Hexagonal Boron Nitride for Efficient and Stable Hydrogenation of Aromatic Amines to Alicyclic Amines, *Ind. Eng. Chem. Res.*, 2023, **62**, 11504-11516.

6 H. Yang, L. Wang, S. Xu, Y. Cao, P. He, J. Chen, Z. Zheng and H. Li, Green and selective hydrogenation of aromatic diamines over the nanosheet $Ru/g-C_3N_4-H_2$ catalyst prepared by ultrasonic assisted impregnation-deposition method, *Green Energy Environ.*, 2022, **7**, 1361-1376.

7 Y. Huang, Y. Ma, Y. Cheng, L. Wang and X. Li, Dimethyl Terephthalate Hydrogenation to Dimethyl Cyclohexanedicarboxylates over Bimetallic Catalysts on Carbon Nanotubes, *Ind. Eng. Chem. Res.*, 2014, **53**, 4604-4613.

8 Z. Wei, Y. Li, J. Wang, H. Li and Y. Wang, Chemoselective hydrogenation of phenol to cyclohexanol using heterogenized cobalt oxide catalysts, *Chinese Chem. Lett.*, 2018, **29**, 815-818.

9 K. Murugesan, T. Senthamarai, A. S. Alshammari, R. M. Altamimi, C. Kreyenschulte, M.-M. Pohl, H. Lund, R. V. Jagadeesh and M. Beller, Cobalt-Nanoparticles Catalyzed Efficient and Selective Hydrogenation of Aromatic Hydrocarbons, *ACS Catal.*, 2019, **9**, 8581-8591.

10 X. Wang, S. Zhu, S. Wang, J. Wang, W. Fan and Y. Lv, Ni nanoparticles entrapped in nickel phyllosilicate for selective hydrogenation of guaiacol to 2-methoxycyclohexanol, *Appl. Catal. A-Gen.*, 2018, **568**, 231-241.